Biomaterials Science

ROYAL SOCIETY OF CHEMISTRY

PAPER

View Article Online
View Journal | View Issue

Cite this: *Biomater. Sci.*, 2023, **11**, 6587

Peptide derived from stromal cell-derived factor 1δ enhances the *in vitro* expression of osteogenic proteins *via* bone marrow stromal cell differentiation and promotes bone formation in *in vivo* models

Jong Keun Seon,[a,b,c] Sree Samanvitha Kuppa,[a,b,c] Ju Yeon Kang,[b,c] Jun Sik Lee,[d] Su A. Park,[e] Taek Rim Yoon,[b] Kyung Soon Park[b] and Hyung Keun Kim *[b,c]

Mesenchymal stem cells (MSCs) rely on chemokines and chemokine receptors to execute their biological and physiological functions. Stromal cell-derived factor-1 (SDF-1) is upregulated in injury sites, where it acts as a chemotactic agent, attracting CXCR4-expressing MSCs, which play a pivotal role in the healing and regeneration of tissue throughout the body. Furthermore, SDF-1 expression has been observed in regions experiencing inflammation-induced bone destruction and fracture sites. In this study, we identified a novel peptide called bone-forming peptide-5 (BFP-5), derived from SDF-1δ, which can promote the osteogenesis of MSCs as well as bone formation and healing. Multipotent bone marrow stromal cells treated with BFP-5 showed enhanced alizarin red S staining and higher alkaline phosphatase (ALP) activity. Moreover, ALP and osterix proteins were more abundantly expressed when cells were treated with BFP-5 than SDF-1α. Histology and microcomputed tomography data at 12 weeks demonstrated that both rabbit and goat models transplanted with polycaprolactone (PCL) scaffolds coated with BFP-5 showed significantly greater bone formation than animals transplanted with PCL scaffolds alone. These findings suggest that BFP-5 could be useful in the development of related therapies for conditions associated with bones.

Received 9th May 2023,
Accepted 6th August 2023

DOI: 10.1039/d3bm00798g

rsc.li/biomaterials-science

1. Introduction

Mesenchymal stem cells (MSCs) are a desirable source for generating new bone tissue in cell-based wound healing processes due to their versatility and ability to differentiate into a wide range of cell types.[1] Several experimental and clinical trials that have attempted to regenerate bones using MSCs have faced significant challenges, such as susceptibility to infection, variable capacity of cells to differentiate in particular *in vivo* circumstances, the expensive nature of *ex vivo* cell manipulation, the limited number of cells that can help with bone formation, and the potential malignant transformation during *ex vivo* cell enlargement.[2–4] Both local MSCs derived from the affected tissue and systemic MSCs participate in the regenerative healing of damaged organs. MSCs in circulation can identify damaged regions of tissue, migrate to the site of injury, and differentiate into tissue-specific components in response to chemokines released by the wounded tissue.[5] Chemokines are a superfamily of small, secreted proteins with four cysteine residues, which form two disulfide links. According to the relative positions of the initial two cysteines, two subfamilies exist: CXC (α) and CC (β).[6–9]

CXCL12, also known as stromal cell-derived factor-1 (SDF-1), is a chemokine belonging to the CXC family, wherein the two initial cysteines are separated by a single intermediate amino acid. SDF-1 is expressed in many tissues, including the bone marrow, liver, kidney, and spleen.[10] It plays many important roles by activating the receptor, CXCR4.[11–13] SDF-1 is expressed by endothelial and stromal cells in the bone marrow, where it functions as a chemoattractant for hemato-

[a]*Department of Biomedical Sciences, Chonnam National University Medical School, Chonnam National University Hwasun Hospital, 322 Seoyang-ro, Hwasun-eup, Jeonnam, 58128, Korea*
[b]*Department of Orthopaedics Surgery, Center for Joint Disease of Chonnam National University Hwasun Hospital, 322 Seoyang-ro, Hwasun-eup, Jeonnam, 519-763, Korea. E-mail: chemokines@naver.com*
[c]*Korea Biomedical Materials and Devices Innovation Research Center of Chonnam National University Hospital, 42, Jebong-ro, Dong-gu, Gwangju, 501-757, Korea*
[d]*Department of Biology, Integrative Biological Sciences & BK21 FOUR educational Research Group for Age-Associated Disorder Control Technology, Immunology Research Lab, College of Natural Sciences, Chosun University, Dong-gu, Gwangju 501-759, Korea*
[e]*Nano Convergence & Manufacturing Systems, Korea Institute of Machinery and Materials (KIMM), Daejon 34103, Korea*

poietic stem cells, promoting their survival and growth after their recruitment to the bone marrow niche.[13,14] The SDF-1/CXCR4 axis plays an imperative part in the biology and physiology of MSCs.[15,16] For the regeneration of organs such as the heart,[17,18] liver,[19] kidney,[20] brain,[21] and skin,[22] SDF-1 must be present at elevated levels near the sites of injury, acting as a potent chemoattractant to recruit circulating or resident CXCR4-expressing MSCs. Furthermore, cardiac[17,18] and brain[21] injuries are more likely to attract circulating mesenchymal stromal and progenitor cells due to the local transport of SDF-1 into damaged tissue. However, the role of the SDF-1/CXCR4 axis in MSC-mediated bone repair has not been elucidated yet. MSCs inhibit SDF-1-mediated osteoclastogenesis in regions of inflammatory bone resorption.[23]

The monomeric form of SDF-1 is found in all living organisms. Alternative splicing gives rise to six different isoforms, namely α, β, γ, δ, ε, and θ, all of which share the initial three exons, but vary from the fourth exon onwards.[24] The C-terminus of SDF-1δ is extended by 50 amino acids, making it more than 50% longer compared with SDF-1α. This additional "tail" may significantly impact the function or activity of SDF-1, or may serve as a binding site for other regulating proteins or cellular components.[24] SDF-1 has the potential to be integrated into scaffolds to promote bone formation. Its effects on cell migration and growth reveal its diverse biological functions. Endothelial progenitor cells sourced from the bone marrow reflect the importance of SDF-1 in angiogenesis.[25] The stimulation of the homing of bone marrow MSCs has implications in the context of bone regeneration.[26]

In this study, a novel bone-forming peptide (BFP) derived from SDF-1δ was synthesized, purified, and investigated for its potential in bone regeneration and tissue repair (Fig. 1). Subsequent analyses revealed osteogenic effects in multipotent bone marrow-derived MSCs and higher activity than SDF-1, providing a proof of concept for this peptide. The efficacy of the peptide in bone regeneration was further assessed in a rabbit tibial defect and a goat cortical defect model. Rabbits are the primary animal models for musculoskeletal research. The weight of goats is analogous to that of adult humans, and their bones have the required size to be employed in the evaluation of human prostheses and implants,[27] therefore both rabbit and goat models were employed in this study. A polycaprolactone (PCL) scaffold, which was proportional in size and diameter to the defect in both the animal models, was printed. Using the PCL scaffold and/or PCL scaffold + BFP-5 as biomimetic bone, an *in vivo* study was conducted over 4, 8, and 12 weeks to examine the biomaterial's osteogenic properties and subsequent bone regeneration. The results were analyzed using microcomputed tomography (CT) and histological examination.

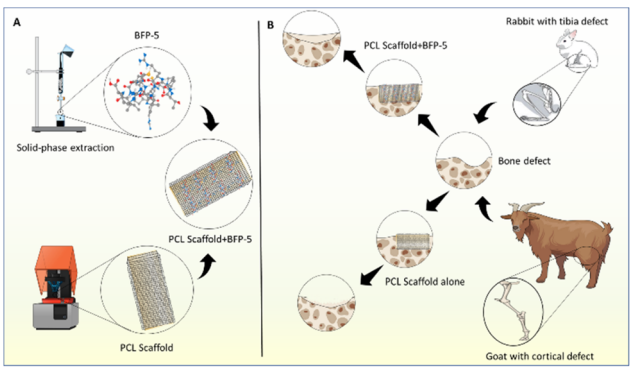

Fig. 1 (A) Schematic of the fabrication of BFP-5 and the PCL scaffold. (B) Diagram illustrating the comparative use of the synthesized scaffold to the treatment of the bone defects in the rabbit and goat model.

2. Materials and methods

2.1. Osteogenic differentiation

The culture conditions for mouse multipotent bone marrow stromal cells (MBSCs) were similar to those reported earlier.[28] MBSCs were obtained from the American Type Culture Collection (ATCC, USA), seeded at a density of 1×10^4 cells per well, and cultured in Dulbecco's Modified Eagle Medium supplemented with 10% fetal bovine serum (Gibco BRL, USA) and antibiotics (Gibco BRL, USA) for 3 days at 37 °C in a humidified 5% CO_2 environment. Experiments were carried out when cells attained 80% confluency. Osteogenic differentiation was initiated by replacing the growth medium with osteogenic differentiation medium (ODM; Dulbecco's Modified Eagle Medium supplemented with 50 μg ml^{-1} ascorbic acid, 10^{-8} M dexamethasone, and 10 mM β-glycerophosphate; all from Sigma-Aldrich, USA) after 3 days. Cultures were maintained in either ODM alone or ODM + BFP-5 (0.01, 0.1, 1, or 10 μg ml^{-1}) for comparison. After 24 h, the cells were examined.

2.2. Synthesis and purification of the BFP-5 peptide

Fluorenylmethoxycarbonyl solid-phase peptide synthesis was performed using ASP48S (Peptron Inc. Daejon, South Korea), and the peptides were purified through reverse-phase high performance liquid chromatography with a Vydac Everest C18 column (250 mm × 22 mm, 10 μm). For elution, a linear gradient of water and acetonitrile (3%–40% [v/v]) containing 0.1% (v/v) trifluoroacetic acid was used. After purification, the peptide's molecular weight was verified by liquid chromatography/mass spectrometry (Agilent HP1100 series, Santa Clara, CA, USA).

2.3. Alizarin red-S staining

Calcium deposits in cells were quantified as described by Chen *et al.*[29] In brief, cell cultures were washed twice with deionized water, fixed for 1 h in ice-cold 70% ethanol, washed twice more, stained for 10 minutes with alizarin red S solution, and gently rinsed under flowing water to remove any residual pigment. Light microscopy images revealed calcium deposits as brilliant red.

2.4. ALP activity assay

ALP activity was assayed in culture medium supplemented with 10% fetal bovine serum, 50 μg ml^{-1} ascorbic acid, 10 mM β-glycerophosphate, and 10^{-8} M dexamethasone. Cells (10–12-passages-old, 80% confluent) were stimulated with 0.01, 0.1, 1 and 10 μg ml^{-1} of BFP-5 and 1 μg ml^{-1} of BFP-1 and SDF-1α for 24 h in 6-well plates, washed twice with phosphate-buffered saline, and incubated with glycine buffer (100 mM glycine, pH 10.5) containing 2 mM $MgCl_2$ and 8 M *p*-nitrophenylphosphate. Absorbance at 405 nm was used to measure the quantity of *p*-nitrophenylphosphate.

2.5. Reverse transcription-polymerase chain reaction (RT-PCR)

The effects of BFP-5 were assessed on the transcription of genes encoding the following proteins using the corresponding primer sets (in brackets): runt-related transcription factor 2 (RUNX2) (5′-ACA AAC AAC CAC AGA ACC ACA AGT-3′, 5′-GTC TCG GTG GCT GGT AGT GA-3′), alkaline phosphatase (ALP) (5′-ACA CCT TGA CTG TGG TTA CTG CTG A-3′;5′-CCT TGT AGC CAG GCC CGT TA-3′), osteopontin (5′-CCA GGT TTC TGA TGA ACA GTA TCC-3′, 5′-ACT TGA CTC ATG GCT GCC CTT T-3′), collagen type I (5′-GGT CGT GGT GCT GCT-3′, 5′-ACC TTT GCC CCC TTC TTT G-3′), DLX5 (5′-CAG CGA CCC TAT GGC GTG TAA CTC-3′, 5′-AGG GGG CGG GGC TCT CTG AAA TGC-3′), osterix (5′-CCT TTC AGC CCC CAA AAC C-3′, 5′-AGC TGT GAA TGG GCT TCT T-3′) and the housekeeping enzyme glyceraldehyde-3-phosphate dehydrogenase (GAPDH) (5′-ATC ACT GCC ACC CAG AAG AC-3′;5′-ATG AGG TCC ACC ACC CTG TT-3′). MBSCs cells grown to 80% confluence on plates with/without BFP-5 were homogenized using TRIzol reagent (Life Technologies, USA). Total RNA was isolated, and 0.5 μg RNA aliquots were reverse-transcribed in 20 μl buffer containing 5× AMV reverse transcriptase; 2.5 μM poly dT; 1 mM each of dATP, dCTP, dGTP, and dTTP; 20 U of RNAse inhibitor; and 20 U of AMV RT. Reverse transcription was performed using the following conditions: initial incubation at room temperature for 10 min and then 42 °C for 15 min, 97 °C for 5 min, and 5 °C for 5 min in a GeneAmp PCR System 2700 (Applied Biosystems, USA). Aliquots of cDNA were amplified in AccuPower® PCR premix (Bioneer Co., Daejeon, South Korea) using the Bioneer gradient thermal cycler system (Daejon, South Korea).

2.6. Western blotting

Whole cell lysates were prepared from MBSCs in 100 μl lysis buffer per well using RIPA Lysis and Extraction Buffer (Thermo Scientific, USA) 1× complete protease inhibitor (Roche Applied Science, Mannheim). The lysates were centrifuged for 10 minutes at 12 000 rpm at 4 °C for 10 min. Protein samples were electrophoresed on a SDS polyacrylamide gel and were transferred onto a polyvinylidene difluoride membrane (Millipore, Billerica, MA, USA). Membranes were washed with TBS/0.1% Tween 20, and then blocked with Difco™ Skim Milk in TBS/0.1% Tween 20 (Amersham Biosciences, USA) for 1 hour at room temperature. Membranes were probed with GAPDH antibodies (Santa Cruz Biotechnology, CA, United States), Anti sp7/osterix antibody (abcam, USA), ALP (abcam, USA), anti-VEGF (abcam, USA) overnight and membranes were washed with TBS/0.1% Tween 20 followed by incubation with horseradish peroxidase conjugated anti-rabbit or anti-mouse secondary antibody (Santa Cruz Biotechnology) for 3 hours. Bands were visualized using an enhanced chemiluminescence detection system (BioRad, CA, United States) and exposed to radiographic film.

2.7. Fabrication of the 3D-printed PCL scaffold and preparation of BFP-5-coated PCL scaffolds

As described in our previous papers, 3D printed PCL scaffolds were created using a 3D rapid prototyping system (labmade system in Korea Institute of Machinery and Materials).[30,31] Initially, a 10 cm × 10 cm PCL scaffold sheet was prepared, which was subsequently cut into appropriate sizes of 5 mm for rabbit defects and 8 mm for goat defects to facilitate *in vivo* implantation.[31,32] For the preparation of BFP-5-coated PCL scaffolds, the 3D-printed PCL scaffolds underwent a series of steps. First, the scaffolds were washed multiple times with double distilled water (DDW) and dried under a nitrogen gas stream. Subsequently, the PCL scaffolds were immersed in 70% ethanol for 30 minutes and washed with phosphate-buffered saline (PBS). The process was followed by the grafting of BFP-5 onto the PCL scaffolds. To ensure the integrity of the peptide, the BFP-5-modified scaffolds were prepared aseptically. The sterilized PCL scaffolds were immersed in a submicron filtered BFP-5 solution, considering the potential susceptibility of the peptide to damage. The immobilization of BFP-5 was achieved by immersing the sterilized PCL scaffolds in the selected concentrations of BFP-5 solution (1 μg ml^{-1} in 10 mM Tris buffer, pH 8.5) while stirring for 24 hours at room temperature. Prior to implantation, the BFP-5-coated scaffolds were briefly rinsed with PBS to remove any unbound peptide.

2.8. Animal experimental design

All animal procedures were performed in conformance with the guidelines of the Ethics Committee of Chonnam National University Medical School and Chonnam National University Hospital (permission number: CNUHIACUC-20032). Skeletally mature male New Zealand white rabbits (age 14–16 weeks, body weight 3.0–3.5 kg) were used to create a 5 mm tibial bone defect (Fig. 2). The rabbits were randomly assigned to one of two groups: group 1, implanted with an empty PCL scaffold, and group 2, implanted with PCL scaffold + BFP-5 (n = 2 per group). Quantitative micro-CT and histology were used to evaluate the rate of bone healing 4, 8, and 12 weeks after surgery. For experiments involving goats, two adult skeletally mature male Korean black goats weighing 35.2 kg and 32.3 kg were used. Their femoral shaft close to the left knee joint was surgically exposed (Fig. 2), an 8 mm-diameter circular cortical bone defect was induced in two places (proximal and distal) at intervals of 3 cm, and the control (PCL scaffold) or test (PCL + BFP-5) scaffolds were implanted on site. Histological and

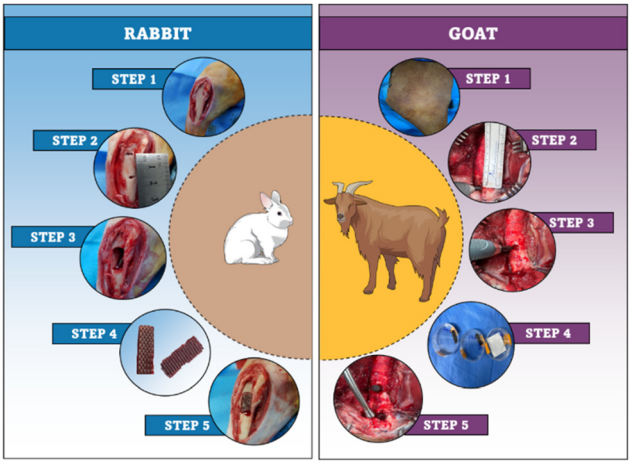

Fig. 2 Surgical procedures involved in bone defect creation in rabbit and goat. Rabbit step 1. Tibia exposition, step 2. Identification of length before bone defect, step 3. From a point 1.5 cm away from the medial tibial plateau, a rectangular cortical bone 5 mm wide and 1.5 cm long was formed using a dental drill and the bone marrow was removed, step 4. The control PCL scaffold and PCL + BFP-5 scaffold was prepared, step 5. The defect was treated using the prepared scaffolds. Goat step 1. The goat was laid in a right lateral recumbency position, and the hair on the left thigh was removed with a hair clipper and disinfected with 70% ethanol and betadine, step 2. The femoral shaft was exposed using a retractor and a longitudinal incision was made on the left posterior thigh about 15 cm, step 3. Cortical bone defects were made 3 cm apart using an 8 mm trephine bur and a micro burr, step 4. The control PCL scaffold and PCL + BFP-5 scaffolds were prepared, step 5. Scaffolds were implanted into the bone defect area.

micro-CT evaluations were performed at 12 weeks after implantation.

2.9. Histological evaluation

Following fixation in 10% neutral-buffered formalin, the tissues were decalcified in 10% EDTA. Using a microtome, 8 μm-wide sections of paraffin-embedded materials were cut, placed on poly-L-lysine-coated microscopy plates, suspended in a water bath at 40 °C, and baked for 2 h at 37 °C. For hematoxylin and eosin staining, the slices were dewaxed in xylene and rehydrated in ethanol solutions of varying concentrations. Hematoxylin and eosin were used to color the nuclei for 5 and 1 min, respectively. The pieces were then cover-slipped and coated in Permount mounting medium.

2.10. Micro-computed tomography analysis

The proximal tibias and femoral shafts that were harvested were scanned in the anterior–posterior, cross-sectional, and lateral planes to assess bone regeneration. Images generated through micro-CT were acquired on the MFR-Polaris-G90 apparatus. The scan was performed at a voltage of 155 kV and a current of 105 mA. To procure section reconstruction visuals, the data view program Skyscan (Kontich, Belgium) was used. CTAn software was deployed for the analysis of both the cortical and trabecular bone regions to establish the regions of interest, which included both the defect sites. A series of images were subsequently aligned.

2.11. Statistical analysis

The data were presented as means ± standard deviations, and analyzed using GraphPad Prism 9 (GraphPad Software, Inc, USA) with one-way analysis of variance. Statistics were deemed significant for *P*-values (*, $^{\#}$ $p < 0.05$, **, $^{\#\#}$ $p < 0.01$, ***, $^{\#\#\#}$ $p < 0.001$, ****, $^{\#\#\#\#}$ $p < 0.0001$).

3. Results

3.1. Synthesis of BFP-5

In this study, we have added a new peptide to the BFP series. We previously reported BFP-4, originating from the immature region of bone morphogenetic protein-7 (BMP-7), to possess bone regeneration capacities.[33] After completing our investigation of BMP-7, we have now directed our attention to the small chemokine SDF-1, a member of the CXC subfamily. The SDF-1/CXCR4 signaling axis has been demonstrated to promote recovery from femoral bone damage by modulating stem cell populations, such as those of mesenchymal and hematopoietic stem cells.[34] Thus, we concentrated our efforts on exploring additional osteogenic peptide sequences from the delta region of SDF-1. A novel peptide with the sequence PPRACPTARALCEIR (Fig. 3), denoted as BFP-5, demonstrated enhanced osteogenic effects in a cell culture system when compared with SDF-1. The full-length BFP-5 peptide was then cloned and registered in the GenBank database (accession number: NP_001171605.1).

3.2. Osteogenic differentiation potential and ALP activity of BFP-5

The osteogenic potential of MBSCs exposed to varying concentrations of BFP-5 was ascertained using alizarin red staining and ALP activity assay. Alizarin red accumulated in a dose-dependent manner, peaking when 1 μg ml^{-1} BFP-5 was administered. It accumulated to a much lower level when 1 μg ml^{-1} of SDF-1α[35] and BFP-1,[31] which are well-recognized for their

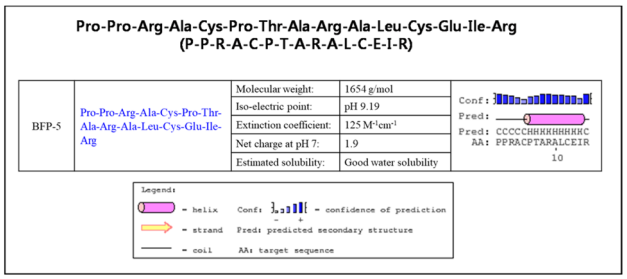

Fig. 3 Synthesis of BFP-5 peptide. The peptide was produced by Fmoc solid-phase peptide synthesis through an automated peptide synthesizer and was further purified by reverse-phase high-performance liquid chromatography. The molecular mass of the purified peptide was determined by means of liquid chromatography/mass spectrometry.

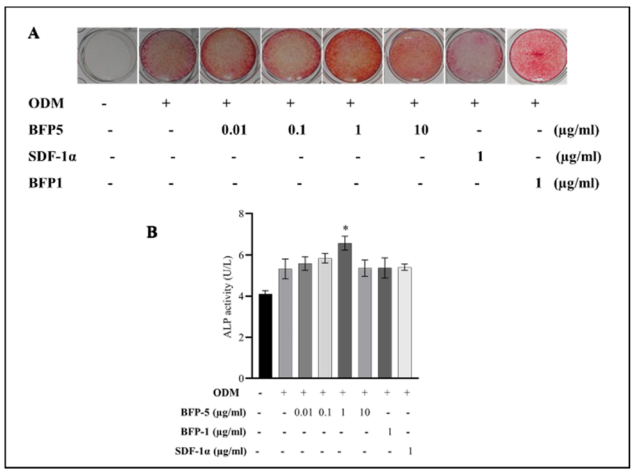

Fig. 4 Osteogenic differentiation potential and ALP activity of BFP-5. (A) Alizarin red stain was administered to evaluate mineralization of MBSCs cells post-treatment with various concentrations of BFP-5. As a baseline, cells were cultivated in ODM or were exposed to the proteins SDF-1α and BFP-1 peptide as representative positive controls. (B) The ALP activity of BFP-5 was assessed in MBSCs at concentrations of 0.01–10 μg ml^{-1}. The ALP activity data represent the mean ± SD from triplicate measurements (* $p < 0.05$ of cells treated with BFP-5 *versus* cells in ODM).

potent osteogenic properties, were administered. Comparatively, alizarin red staining was noticeably diminished in the 10 μg ml^{-1} group (Fig. 4A). Similarly, 1 μg ml^{-1} BFP-5 considerably augmented ALP activity in comparison to ODM (Fig. 4B). Although 10 μg ml^{-1} BFP-5 significantly promoted osteogenic differentiation compared with the negative and positive controls, its effect was milder than that of 1 μg ml^{-1} BFP-5. Subsequently, we used 1 μg ml^{-1} BFP-5 in all further experiments.

3.3. BFP-5 increases osteogenic differentiation markers in MBSCs

To investigate the molecular profiles associated with morphological changes during early osteogenic differentiation induced by BFP-5, we estimated the expression of RUNX2, osterix, ALP, DLX5, collagen type I, and the late osteogenic marker osteopontin using reverse transcription-PCR. The levels of all osteogenic markers increased markedly upon treatment with BFP-5 compared with the untreated control, and the ODM-, SDF-1α-, and BFP-1-induced groups (Fig. 5A). The mRNA and protein expression levels of ALP and osterix concurred (Fig. 6A). On the basis of elevated ALP expression, we further investigated the protein expression of VEGF, a crucial marker implicated in bone homeostasis that promotes ALP activity and mineralization.[36,37] A comparison between cells stimulated with BFP-5 and those stimulated with VEGF, fibroblast growth factor, SDF-1α, and SDF-1γ revealed an increased expression of VEGF in the former, suggesting that BFP-5 can induce osteogenic differentiation markers in MBSCs (Fig. 6B).

3.4. BFP-5 promotes tissue regeneration in both rabbits and goats

Following implantation of PCL and PCL + BFP-5 scaffolds into the rabbit bone defect, all postoperative progressions were unremarkable. No adverse outcomes (edema, erythema, sepsis, separation of incision edges, or exposure of the operative site) were noted over the entire postoperative course. At 4 weeks, individual histopathological analyses depicted infiltration of cells at the periphery of the scaffold, and minimal new tissue within the scaffold. At this timepoint, the two groups did not differ significantly in terms of the quantity of new tissue.

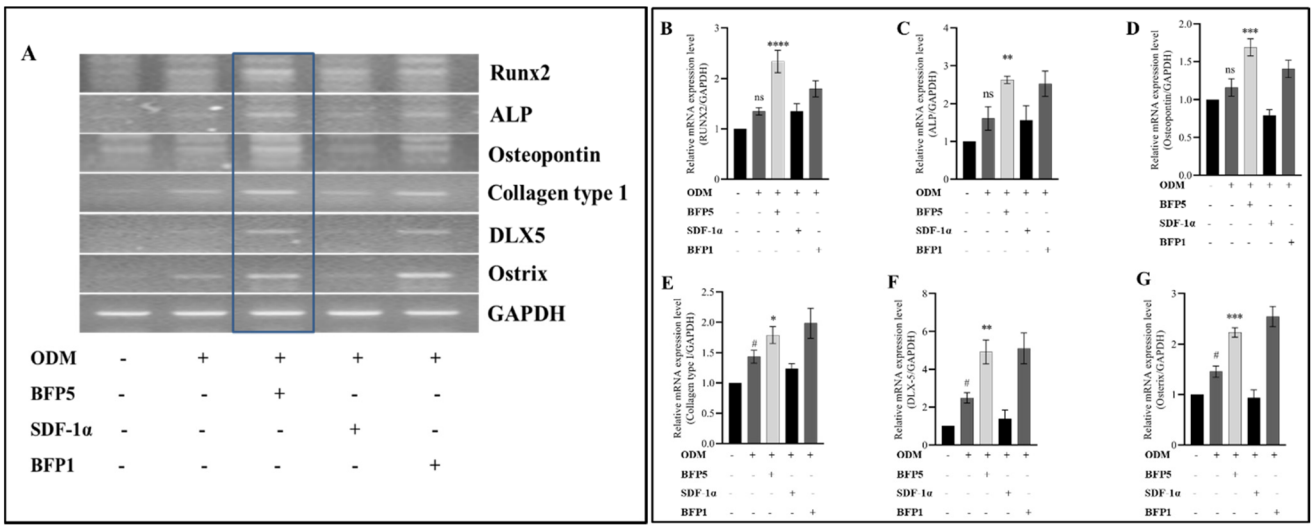

Fig. 5 BFP-5 increases osteogenic differentiation markers in MBSCs. (A) RT-PCR analysis for the osteogenic differentiation gene marker of MSBCs following treatment with BFP-5. Relative mRNA expression level for (B) RUNX2, (C) ALP, (D) osteopontin, (E) collagen type I, (F) DLX-5, and (G) osterix. The above data represent the mean ± SD from triplicate measurements (# $p < 0.05$ ODM *versus* negative control; * $p < 0.05$, ** $p < 0.01$, *** $p < 0.001$, **** $p < 0.0001$ of cells treated with BFP-5 *versus* cells in ODM).

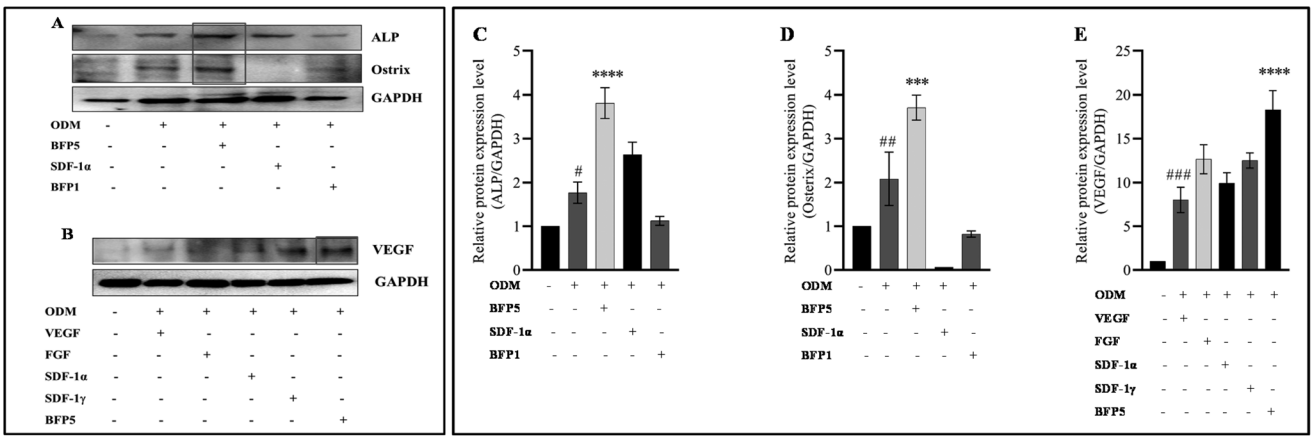

Fig. 6 Western blotting analysis of expression of (A) ALP and Osterix, and (B) VEGF after BFP-5 treatment. Relative protein expression level for (C) ALP, (D) osterix, (E) VEGF. The above data represent the mean ± SD from triplicate measurements (# $p < 0.05$, ## $p < 0.01$, ### $p < 0.001$ ODM *versus* negative control, *** $p < 0.001$, **** $p < 0.0001$ of cells treated with BFP-5 *versus* cells in ODM).

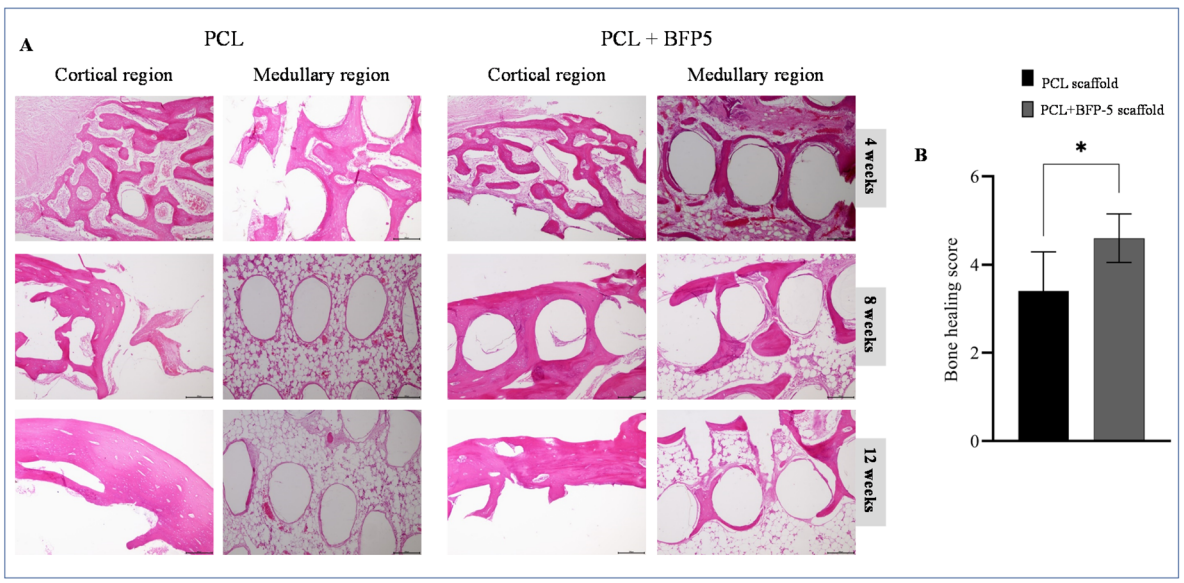

Fig. 7 Histological findings of PCL and PCL + BFP-5 scaffold groups 4, 8, and 12 weeks after surgery in rabbits. The results showed a more advanced progression of osteogenesis and calcification in the PCL + BFP-5 scaffold group when compared to the PCL group in rabbits. No evidence of any inflammatory cells was observed in any groups. (B) Statistical analysis of the histological sections of bone healing in each group 12 weeks post-operation. Data were expressed as mean ± SD ($n = 2$). Significantly different (*$p < 0.05$) from PCL alone.

At 8 and 12 weeks, cells and tissue had markedly grown compared with that at 4 weeks (Fig. 7A). The delineation between the materials and the enveloping tissues became progressively ambiguous, with new tissues developing within the scaffold as it degraded. Within the medullary region of the subcortical area of the scaffold implantation, both groups demonstrated equivalent degrees of bone generation at 4 and 8 weeks. At 12 weeks, a greater amount of newly formed bone had developed in the porosity of the scaffold in the PCL + BFP-5 group compared with the PCL group. A mesh-like pattern of skeletal columns had formed in the area of active ossification in the PCL + BFP-5 group. A combination of woven and lamellar bone was observed in the sample, and a significant difference was noted overall compared with the control PCL group (Fig. 7A). In the tissue scoring assessment, the sum of the bone regeneration scores from the cortical bone and medullary canal area of the PCL and PCL + BFP-5 scaffolds were 3.4 and 4.6, respectively, demonstrating a greater degree of bone regeneration in the PCL + BFP-5 group, and confirming the hypothesis (Fig. 7B).

Based on the outcomes of the rabbit model, we also evaluated the goat model at 12 weeks. At 12 weeks post-implantation, histological examination of goats revealed no evidence of inflammation or foreign body response at the implantation

sites in both the PCL and PCL + BFP-5 groups. Tissue slide microscopy revealed that most of the PCL scaffolds in the implanted cortical bone area exhibited a sparse fibrous network structure. The defect was populated with soft and connective tissue, while the interior was being traversed by the newly formed bone. Until date, no entity displaying a tangible

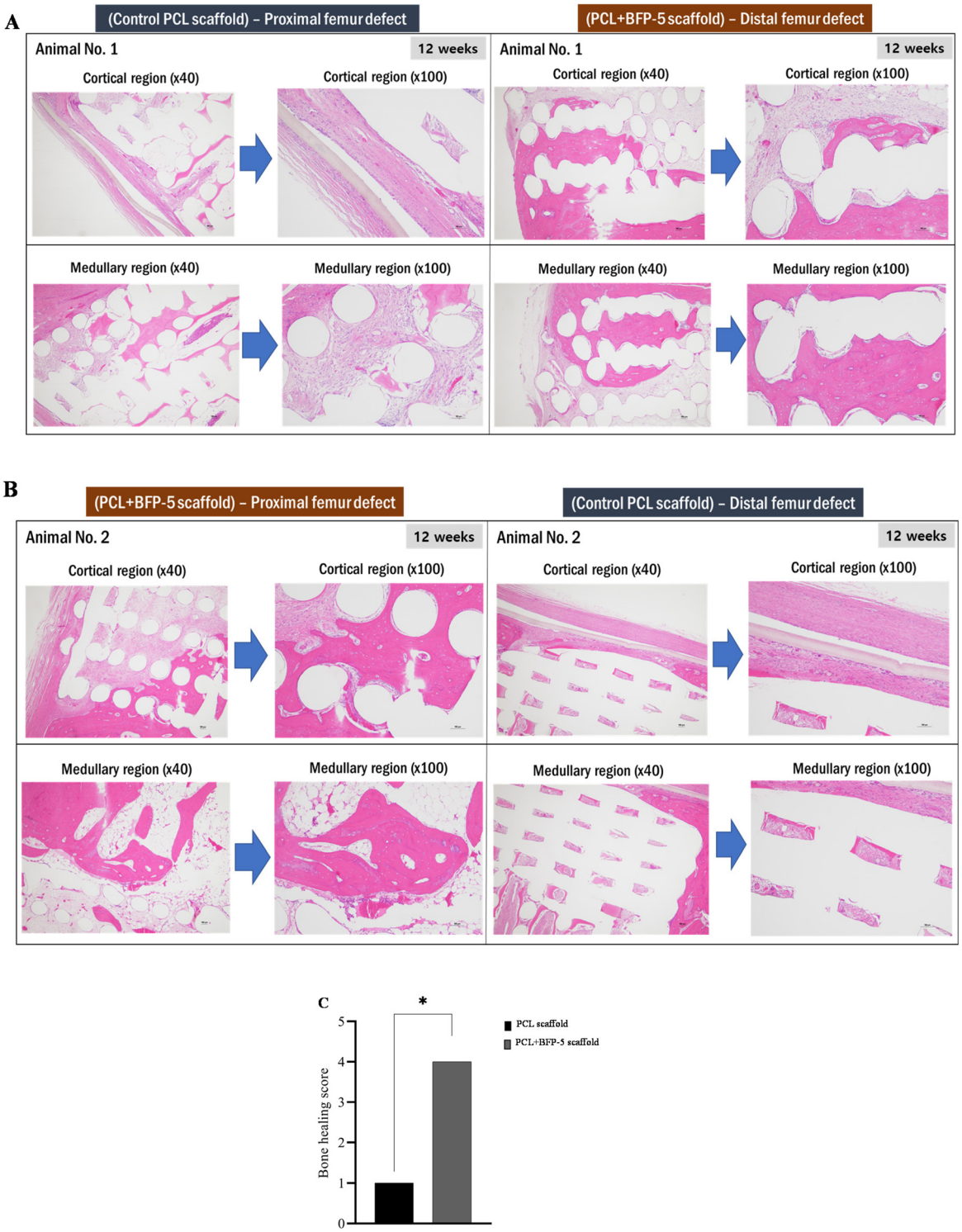

Fig. 8 Histological findings of PCL and PCL + BFP-5 scaffold groups 4, 8, and 12 weeks after surgery in rabbits. The results showed a more advanced progression of osteogenesis and calcification in the PCL + BFP-5 scaffold group when compared to the PCL group in rabbits. No evidence of any inflammatory cells was observed in any groups. (B) Statistical analysis of the histological sections of bone healing in each group 12 weeks post-operation. Data were expressed as mean ± SD (n = 2). Significantly different (*p < 0.05) from PCL alone.

osseous protective effect has been identified. Herein, the BFP-5-coated PCL scaffold group displayed a decrease in the amount of connective tissue. The construction of the scaffold was primarily due to the organic connection between the formation of the trabecular bone and the increase in the bony structure on the marginal edges. Compared with the PCL scaffold group, the PCL + BFP-5 scaffold group exhibited significant differences. The augmentation of new bone and the action of bone incorporation in the scaffold lattice environment were more conspicuous in the cortical bone region than in the medullary hollow region. The PCL + BFP-5 scaffold group held a preponderant influence. In the tissue scoring assessment, the sum of the bone regeneration scores from the cortical bone and medullary canal area were 4.0 and 1.0 for the PCL + BFP-5 and the PCL scaffold groups, respectively, demonstrating a greater degree of bone regeneration in the former, and confirming the hypothesis (Fig. 8C).

3.5. BFP-5 promotes bone regeneration

Micro-CT analysis was used to acquire anterior–posterior views of the tibias of rabbits in each group. At 12 weeks, the comparison between cross-sectional and anterior–posterior views revealed that the group with BFP-5 showed greater regeneration in the cortical bone than the group without (Fig. 9A). Ascertaining the disparity in bone regrowth in the medullary region was more challenging because the graft material at the lesion site had not disintegrated yet. An assessment of the three-dimensional structural features of the two scaffolds revealed values of 40.84, 5.69, 0.40, 0.14, and 1.32 for bone volume (BV), bone volume ratio (BV/TV), trabecular thickness (Tb.Th), trabecular number (Tb.N), and bone mineral density (BMD), respectively, for the PCL + BFP-5 scaffold, and 23.37, 3.38, 0.39, 0.09, and 1.54, respectively, for the PCL scaffold, affirming the superior bone regeneration capacity of PCL + BFP-5 in rabbits (Fig. 9B–F).

In goats, the micro-CT image revealed a cortical bone defect window of the distal implantation in the PCL scaffold group. In the proximal region where the PCL + BFP-5 group was implanted, new bone formation was minimal, and the newly formed bone was not completely covered (Fig. 10B). The density of the newly formed bone can be assessed by comparing the transverse and sagittal images relative to the cortical bone in the central defect window (Fig. 10A). The BV, BV/TV, Tb.Th, Tb.N, and BMD of the bone trabeculae in the PCL + BFP-5 and PCL scaffold implantations were measured to be 78.90, 28.26, 0.54, 0.52, and 1.70, and 45.23, 14.37, 0.47, 0.29, and 1.76, respectively (Fig. 10C–G), further corroborating the conclusion that the PCL + BFP-5 scaffold demonstrated higher bone regeneration than the control PCL scaffold.

4. Discussion

The most frequent orthopaedic condition following unintentional damage is fracture. The frequency of severe fractures has considerably risen with the fast growth of society. The two main methods used to repair broken bones—intramembranous and endochondral osteogenesis—utilize MSCs, which are directed to develop into osteoblasts and ultimately into bone tissue.[38] SDF-1 acts as a chemoattractant to draw circulating or localized CXCR4-expressing MSCs to the sites of bone fractures to promote bone healing.[39]

The splice variants SDF-1α and SDF-1δ exhibit analogous amino acid sequences. The 3′ untranslated region and polyade-

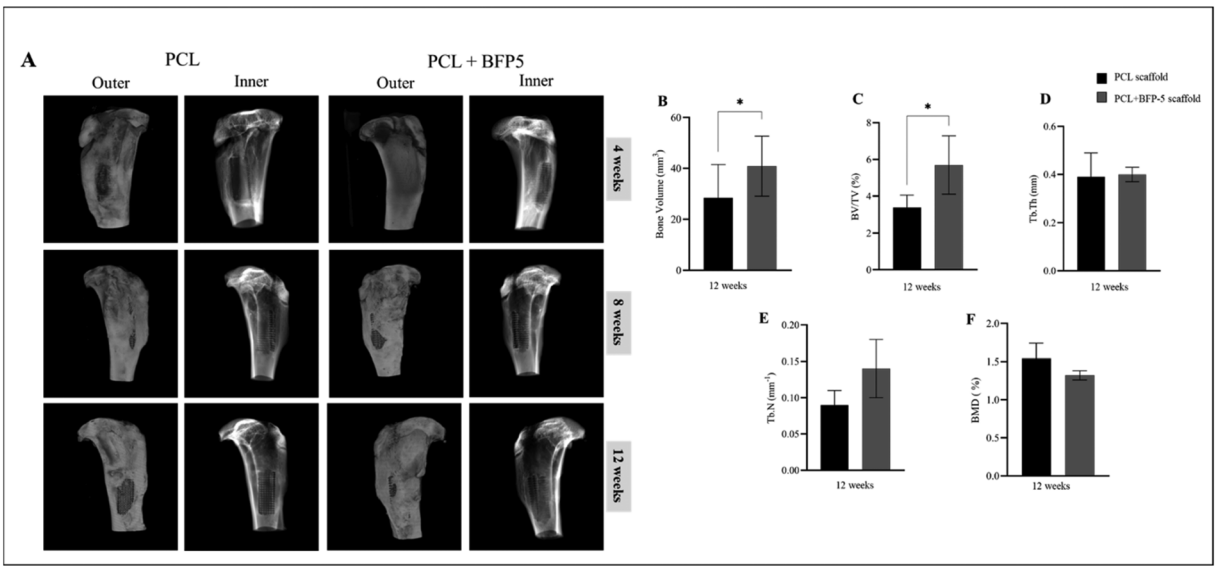

Fig. 9 (A) Representative micro-CT images of rabbit outer and inner bone defect regions after treatment with PCL and PCL + BFP-5 at 4, 8, and 12-weeks post-implantation in rabbits. Quantification of bone regeneration in rabbit (B) bone volume (BV) (C) bone volume per total volume (BV/TV), (D) trabecular thickness (Tb.Th.), (E) trabecular number (Tb.N.), and (F) bone mineral density (BMD), as measured by micro-CT. The values shown are the mean ± SD (n = 2) Significantly different (*p < 0.05) from PCL alone.

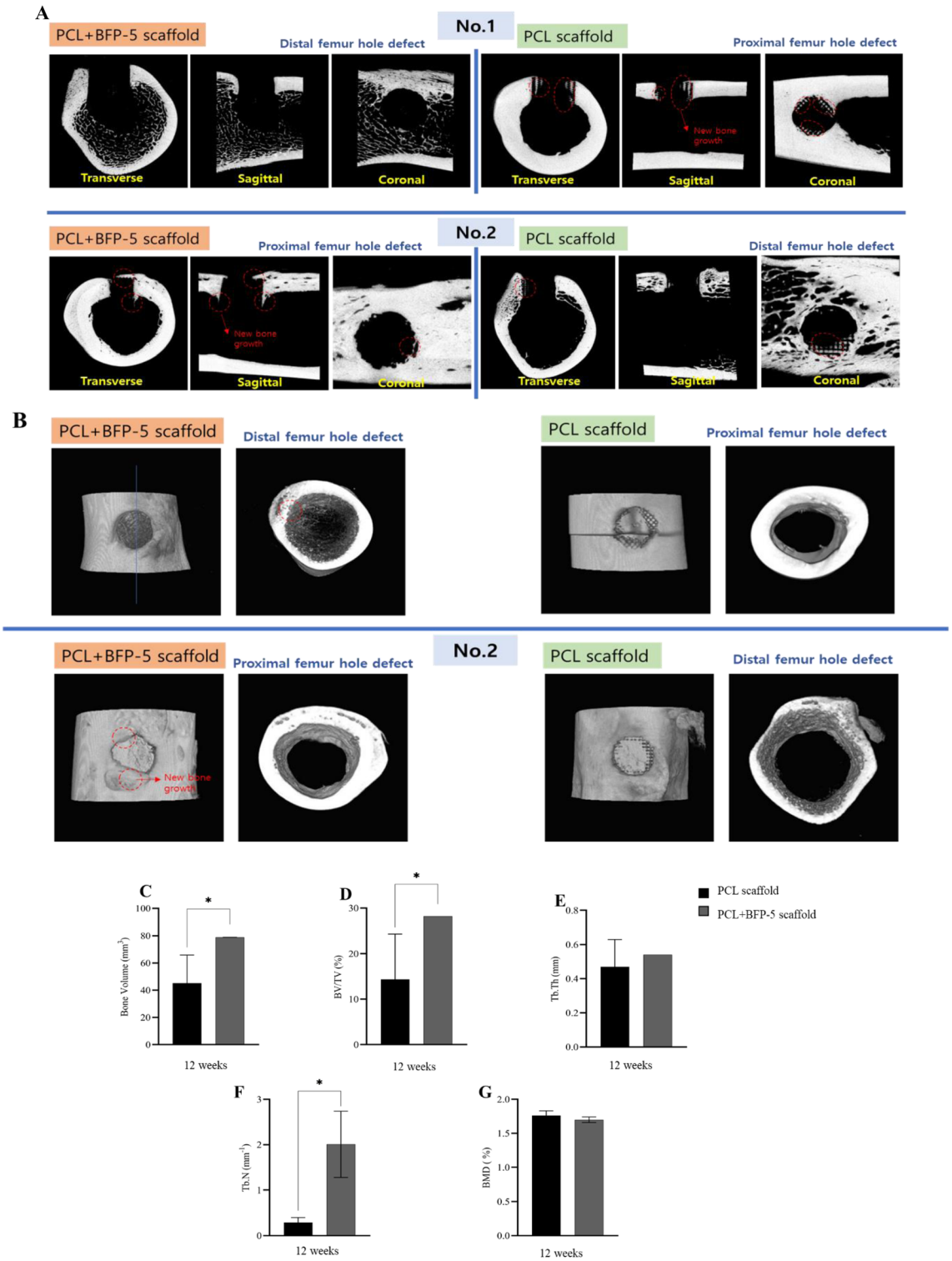

Fig. 10 (A) 2D-image evaluation test for bone regeneration effect of PCL + BFP-5 group and PCL scaffold group for 12 weeks in cortical bone defect model of goat femur shaft (the red markings indicate new bone growth). (B) 3D-image evaluation test of the bone regeneration effect of the PCL + BFP-5 group and PCL scaffold group 12 weeks in the cortical bone defect model of the femur of the goat. Quantification of bone regeneration in goat (C) bone volume (BV) (D) bone volume per total volume (BV/TV), (E) trabecular thickness (Tb.Th.), (F) trabecular number (Tb.N.), and (G) bone mineral density (BMD), as measured by micro-CT. The values shown are the mean ± SD (n = 2) Significantly different (*p < 0.05) from PCL alone.

nylation signal sequence of human SDF-1δ are consistent with those of human SDF-1α. The inferred amino acid sequence of human SDF-1δ was calculated to be 140-residues-long, the first 89 being identical to those of SDF-1α, while the C-terminal 51 residues being a unique additional feature.[40] The C-terminal regions of the novel SDF-1 variants differ from that of SDF-1α by a limited number of amino acid substitutions.[24] Given their sequence similarity, SDF-1δ was hypothesized to possess the same reparative and regenerative attributes as SDF-1α. Thus, this research aimed to explore the effects of an SDF-1δ-derived BFP on the osteogenic differentiation of MBSCs, tissue regeneration, and bone repair.

Previously identified BFPs originating from mature BMPs have been recognized to exert osteogenic effects; however, we have ascertained that peptide sequences of SDF-1δ can also exert similar effects. The capability of BFP-4 to promote osteogenic properties and facilitate bone formation has been demonstrated previously. This research aimed to identify novel peptides capable of enhancing the effectiveness of bone regeneration therapies, and to maximize their economic potential. In the present study, we not only established the osteogenic potential of the newly discovered BFP-5 but also demonstrated its superior bone formation capacity compared with SDF-1α. In addition, BFP-5 stimulated a greater degree of osteogenic differentiation and bone formation than BFP-1 at the same concentration. Furthermore, the implantation of BFP-5-coated scaffolds promoted the healing of critical-sized bone defects, indicating that BFP-5 is a promising biomaterial for bone tissue engineering.

This study evaluated the ability of BFP-5 to induce osteogenic differentiation in MBSCs under *in vitro* controlled conditions. MBSCs possess the remarkable capacity to differentiate into osteogenic, fibroblastic, myogenic, and adipogenic cells. This study utilized MBSCs to explore the osteoinductive properties of BFP-5. The differentiation of MBSCs to osteoblasts was confirmed through alizarin red staining and ALP activity assay. Of all concentrations, 1 μg ml^{-1} of BFP-5 elicited a stronger response in the two confirmatory tests. Higher concentrations of peptide (10 μg ml^{-1}) tend to form self-assembled aggregates, which may limit its osteogenic differentiation capacity. Consequently, 1 μg ml^{-1} of the peptide was chosen for further experimentation.

The differentiation of osteoblasts is intricate and is modulated by various vital components and signaling pathways. BFP-5 increased the transcription of RUNX2,[41] widely regarded as the regulator of osteogenic differentiation. ALP, which is essential for mineralization of the extracellular matrix (ECM), was also increased.[42] Additionally, both collagen type I, the primary constituent of the organic portion of the ECM, and osteopontin, a non-collagenous bone ECM protein, were increased. They have previously been used as indicators for osteogenic differentiation.[43] Further, the expression of osterix and DLX-5, which are essential for both skeletogenesis and osteoblast differentiation, was significantly higher compared with that in SDF-1α-treated cells in ODM.[44] The results of BFP-5 were comparable to those of BFP-1, consequently prompting a comparison between the two. Subsequently, the mRNA expression levels of the respective osteogenic markers induced by BFP-5 were found to be consistent with those induced by BFP-1. The translation of osteogenic markers (ALP and osterix) was also elevated. BFP-5 treatment increased the activity of osteogenic markers, such as VEGF, in MBSCs. VEGF has been demonstrated to play a multifunctional role, promoting endothelial cell migration and proliferation, as well as the regulation of osteogenic growth factors, thus stimulating osteogenesis.[45] Given the interdependent nature of angiogenesis and osteogenesis, they must operate in unison for physiological bone function to be realized. Vascular alterations have been demonstrated to significantly hinder physiological bone healing processes, manifesting as osteonecrosis, osteoporosis, and non-union fractures.[46] MBSCs were exposed *in vitro* to several angiogenesis-stimulating agents (*e.g.*, fibroblast growth factor and VEGF), as well as SDF-1α and SDF-1γ, which are known to attract endothelial progenitor cells to ischemic peripheral tissues besides inducing angiogenesis,[47] to evaluate the angiogenic effects of BFP-5. BFP-5 upregulated VEGF expression when compared with the other potent inducers.

After establishing the capability of BFP-5 to induce osteogenesis in MBSCs, we aimed to extensively evaluate its potential to generate new bone. Bone regeneration involves the chemotactic movement of MSCs to the area of defect and subsequent morphological developments of migration, differentiation, and proliferation. Bone formation typically involves the uptake of the test material by osteoclasts and the subsequent differentiation and replication of osteoblasts. Bone repair culminates with the bone remodeling phase, which includes the formation of the bone marrow. In this investigation, two animal models were employed to assess bone regeneration. First, the rabbit tibial defect model was employed to evaluate the *in vivo* regeneration of bone when using a PCL scaffold coated with BFP-5. Partial restoration of cortical defects was observed in both groups. The groups employing BFP-5 showed a noteworthy enhancement in cortical bone mass when compared with the control group. The findings of this research suggest that although PCL on its own has the capacity to induce bone growth, a more pronounced osteoinductive effect is achieved when the scaffold is coated with BFP-5. At 12 weeks, a significantly high bone healing score of both cortical and medullary bone areas was observed in the PCL + BFP-5 group with regards to bone strength. The results of this study indicate that BFP-5 promotes bone tissue regeneration in rabbits.

Similarly, in goats, at 12 weeks, histologic assessment revealed no indications of inflammation or foreign body reactions at the implantation sites of the scaffolds. In the control group, in the region of the cortical bone defect where the PCL scaffold was implanted, the new bone was uncovered and largely observed to be a connective tissue flap. The rate of bone regeneration and deposition between scaffold particles within the bone marrow cavity was very slow. However, although the PCL + BFP-5 scaffold did not demonstrate full bone growth, the new bone was both biocompatible and

capable of progressing. New bone columns developed concomitantly, and the bone margin of the lesion as well as in the intramedullary area of the scaffolding was restored. According to previous investigations using the goat model,[32] higher trabecular BV is associated with increased bone strength. With regards to the microscopic architecture of the trabecular bone, increased bone thickness correlates with increased bone strength. Trabecular bone with a lower complexity and more plate-shape tends to be more prevalent than a rod-shaped bone. In the autopsy specimens taken after 12 weeks, the PCL + BFP-5 group displayed a significantly increased BV compared with the PCL group, and higher relative values of BV/TV, Tb. Th, and Tb.N. BMD, on the other hand, indicated a slight downward trend. The bone index analyses revealed no statistically significant difference between the groups, likely attributable to the limited sample size; nevertheless, the PCL + BFP-5 group generally demonstrated better bone-related indicators in comparison to the control PCL group. The results of this experiment showed that the bone regeneration effect of the experimental PCL + BFP-5 group was superior to that of the control PCL group due to increased deposition of bone tissue. We hypothesize that the application of BFP-5-coated scaffolds stimulates the activation of the SDF-1/CXCR4 axis, which is essential as a potent chemoattractant for recruiting circulating or resident MSCs expressing CXCR4. This mechanism of recruitment may contribute to the upregulation of osteogenesis in neighbouring host cells.[48] The enhanced healing response observed may have resulted from the preferential binding and recruitment of osteoprogenitor cells within or around the defect site, or from an increase in the differentiation of undifferentiated cells bound to BFP-5 on the scaffold.

5. Conclusions

To conclude, we present a new peptide (BFP-5) with the capability to stimulate the osteogenic differentiation of MBSCs. A concentration of 1 μg ml^{-1} BFP-5 induced an osteogenic response, while higher concentrations significantly impeded osteogenic differentiation. The results of our study prove that BFP-5 can notably stimulate the osteogenic differentiation of MBSCs, and the transplantation of PCL + BFP-5 scaffolds into rabbit and goat animal models can result in greater bone tissue formation and repair. The BFP-5 biomaterial holds substantial promise for bone tissue engineering.

Ethics statement

The animal study was reviewed and approved by the Ethics Committee of Chonnam National University Medical School and Chonnam National University Hospital (permission number: CNUHIACUC-20032).

Author contributions

Jong Keun Seon: Conceptualization, methodology, investigation, funding acquisition, Sree Samanvitha Kuppa: Data curation, methodology, investigation, analysis and interpretation, writing – original draft, writing – review & editing, Ju Yeon Kang: Methodology, Investigation, Jun Sik Lee: Conceptualization, methodology, visualization, Su A Park, Taek Rim Yoon and Kyung Soon Park: Methodology, investigation, Hyung Keun Kim: Conceptualization, methodology, investigation, review, funding acquisition.

Conflicts of interest

The authors declare no known competing interests.

Acknowledgements

This research was supported by the National Research Foundation of Korea (NRF) grant (No. 2017R1A2B4008676).

References

1 E. L. Herzog, L. Chai and D. S. Krause, Plasticity of Marrow-Derived Stem Cells, *Blood*, 2003, **102**, 3483–3493, DOI: 10.1182/blood-2003-05-1664.
2 M. Gosset, F. Berenbaum, S. Thirion and C. Jacques, Primary Culture and Phenotyping of Murine Chondrocytes, *Nat. Protoc.*, 2008, **3**, 1253–1260, DOI: 10.1038/nprot.2008.95.
3 P. Hernigou, Percutaneous Autologous Bone-Marrow Grafting for Nonunions Influence of the Number and Concentration of Progenitor Cells, *J. Bone Jt. Surg.*, 2005, **87**, 1430, DOI: 10.2106/JBJS.D.02215.
4 M. Kucia and M. Z. Ratajczak, Stem Cells as a Two Edged Sword–from Regeneration to Tumor Formation, *J. Physiol. Pharmacol.*, 2006, **57**(Suppl 7), 5–16.
5 W.-C. Shyu, Homing Genes, Cell Therapy and Stroke, *Front. Biosci.*, 2006, **11**, 899, DOI: 10.2741/1846.
6 F. Sallusto and M. Baggiolini, Chemokines and Leukocyte Traffic, *Nat. Immunol.*, 2008, **9**, 949–952, DOI: 10.1038/ni.f.214.
7 F. Melchers, A. G. Rolink and C. Schaniel, The Role of Chemokines in Regulating Cell Migration during Humoral Immune Responses, *Cell*, 1999, **99**, 351–354, DOI: 10.1016/S0092-8674(00)81521-4.
8 C. Murdoch and A. Finn, Chemokine Receptors and Their Role in Inflammation and Infectious Diseases, *Blood*, 2000, **95**, 3032–3043, DOI: 10.1182/blood.V95.10.3032.010k17_3032_3043.
9 A. Zlotnik and O. Yoshie, Chemokines: A New Classification System and Their Role in Immunity, *Immunity*, 2000, **12**, 121–127, DOI: 10.1016/S1074-7613(00)80165-X.

10 A. J. Schrader, O. Lechner, M. Templin, K. E. J. Dittmar, S. Machtens, M. Mengel, M. Probst-Kepper, A. Franzke, T. Wollensak, P. Gatzlaff, *et al.*, CXCR4/CXCL12 Expression and Signalling in Kidney Cancer, *Br. J. Cancer*, 2002, **86**, 1250–1256, DOI: 10.1038/sj.bjc.6600221.

11 T. Nagasawa, H. Kikutani and T. Kishimoto, Molecular Cloning and Structure of a Pre-B-Cell Growth-Stimulating Factor, *Proc. Natl. Acad. Sci. U. S. A.*, 1994, **91**, 2305–2309, DOI: 10.1073/pnas.91.6.2305.

12 C. C. Bleul, M. Farzan, H. Choe, C. Parolin, I. Clark-Lewis, J. Sodroski and T. A. Springer, The Lymphocyte Chemoattractant SDF-1 Is a Ligand for LESTR/Fusin and Blocks HIV-1 Entry, *Nature*, 1996, **382**, 829–833, DOI: 10.1038/382829a0.

13 Y. Feng, C. C. Broder, P. E. Kennedy and E. A. Berger, HIV-1 Entry Cofactor: Functional CDNA Cloning of a Seven-Transmembrane, G Protein-Coupled Receptor, *Science*, 1996, **272**, 872–877, DOI: 10.1126/science.272.5263.872.

14 J.-J. Lataillade, D. Clay, C. Dupuy, S. Rigal, C. Jasmin, P. Bourin and M.-C. Bousse-Kerdilès, Le Chemokine SDF-1 Enhances Circulating CD34+ Cell Proliferation in Synergy with Cytokines: Possible Role in Progenitor Survival, *Blood*, 2000, **95**, 756–768, DOI: 10.1182/blood.V95.3.756.

15 R. F. Wynn, C. A. Hart, C. Corradi-Perini, L. O'Neill, C. A. Evans, J. E. Wraith, L. J. Fairbairn and I. Bellantuono, A Small Proportion of Mesenchymal Stem Cells Strongly Expresses Functionally Active CXCR4 Receptor Capable of Promoting Migration to Bone Marrow, *Blood*, 2004, **104**, 2643–2645, DOI: 10.1182/blood-2004-02-0526.

16 A. Dar, P. Goichberg, V. Shinder, A. Kalinkovich, O. Kollet, N. Netzer, R. Margalit, M. Zsak, A. Nagler, I. Hardan, *et al.*, Chemokine Receptor CXCR4-Dependent Internalization and Resecretion of Functional Chemokine SDF-1 by Bone Marrow Endothelial and Stromal Cells, *Nat. Immunol.*, 2005, **6**, 1038–1046, DOI: 10.1038/ni1251.

17 J. D. Abbott, Y. Huang, D. Liu, R. Hickey, D. S. Krause and F. J. Giordano, Stromal Cell–Derived Factor-1α Plays a Critical Role in Stem Cell Recruitment to the Heart After Myocardial Infarction but Is Not Sufficient to Induce Homing in the Absence of Injury, *Circulation*, 2004, **110**, 3300–3305, DOI: 10.1161/01.CIR.0000147780.30124.CF.

18 J. Ma, J. Ge, S. Zhang, A. Sun, J. Shen, L. Chen, K. Wang and Y. Zou, Time Course of Myocardial Stromal Cell Derived Factor 1 Expression and Beneficial Effects of Intravenously Administered Bone Marrow Stem Cells in Rats with Experimental Myocardial Infarction, *Basic Res. Cardiol.*, 2005, **100**, 217–223, DOI: 10.1007/s00395-005-0521-z.

19 M. Kucia, Tissue-Specific Muscle, Neural and Liver Stem/Progenitor Cells Reside in the Bone Marrow, Respond to an SDF-1 Gradient and Are Mobilized into Peripheral Blood during Stress and Tissue Injury, *Blood Cells, Mol., Dis.*, 2004, **32**, 52–57, DOI: 10.1016/j.bcmd.2003.09.025.

20 F. Tögel, J. Isaac, Z. Hu, K. Weiss and C. Westenfelder, Renal SDF-1 Signals Mobilization and Homing of CXCR4-Positive Cells to the Kidney after Ischemic Injury, *Kidney Int.*, 2005, **67**, 1772–1784, DOI: 10.1111/j.1523-1755.2005.00275.x.

21 J. F. Ji, B. P. He, S. T. Dheen and S. S. W. Tay, Interactions of Chemokines and Chemokine Receptors Mediate the Migration of Mesenchymal Stem Cells to the Impaired Site in the Brain After Hypoglossal Nerve Injury, *Stem Cells*, 2004, **22**, 415–427, DOI: 10.1634/stemcells.22-3-415.

22 D. J. Ceradini, A. R. Kulkarni, M. J. Callaghan, O. M. Tepper, N. Bastidas, M. E. Kleinman, J. M. Capla, R. D. Galiano, J. P. Levine and G. C. Gurtner, Progenitor Cell Trafficking Is Regulated by Hypoxic Gradients through HIF-1 Induction of SDF-1, *Nat. Med.*, 2004, **10**, 858–864, DOI: 10.1038/nm1075.

23 T. Takano, Y.-J. Li, A. Kukita, T. Yamaza, Y. Ayukawa, K. Moriyama, N. Uehara, H. Nomiyama, K. Koyano and T. Kukita, Mesenchymal Stem Cells Markedly Suppress Inflammatory Bone Destruction in Rats with Adjuvant-Induced Arthritis, *Lab. Invest.*, 2014, **94**, 286–296, DOI: 10.1038/labinvest.2013.152.

24 L. Yu, J. Cecil, S.-B. Peng, J. Schrementi, S. Kovacevic, D. Paul, E. W. Su and J. Wang, Identification and Expression of Novel Isoforms of Human Stromal Cell-Derived Factor 1, *Gene*, 2006, **374**, 174–179, DOI: 10.1016/j.gene.2006.02.001.

25 A. Lauer, P. Wolf, D. Mehler, H. Götz, M. Rüzgar, A. Baranowski, D. Henrich, P. M. Rommens and U. Ritz, Biofabrication of SDF-1 Functionalized 3D-Printed Cell-Free Scaffolds for Bone Tissue Regeneration, *Int. J. Mol. Sci.*, 2020, **21**, 2175, DOI: 10.3390/ijms21062175.

26 S.-J. Zhang, X.-Y. Song, M. He and S.-B. Yu, Effect of TGF-B1/SDF-1/CXCR4 Signal on BM-MSCs Homing in Rat Heart of Ischemia/Perfusion Injury, *Eur. Rev. Med. Pharmacol. Sci.*, 2016, **20**, 899–905.

27 Y. Li, S.-K. Chen, L. Li, L. Qin, X.-L. Wang and Y.-X. Lai, Bone Defect Animal Models for Testing Efficacy of Bone Substitute Biomaterials, *J. Orthop. Transl.*, 2015, **3**, 95–104, DOI: 10.1016/j.jot.2015.05.002.

28 G. A. Dahir, Q. Cui, P. Anderson, C. Simon, C. Joyner, J. T. Triffitt and G. Balian, Pluripotential Mesenchymal Cells Repopulate Bone Marrow and Retain Osteogenic Properties, *Clin. Orthop. Relat. Res.*, 2000, **379**, S134–S145, DOI: 10.1097/00003086-200010001-00018.

29 C.-H. Chen, M.-L. Ho, J.-K. Chang, S.-H. Hung and G.-J. Wang, Green Tea Catechin Enhances Osteogenesis in a Bone Marrow Mesenchymal Stem Cell Line, *Osteoporosis Int.*, 2005, **16**, 2039–2045, DOI: 10.1007/s00198-005-1995-0.

30 E. Y. Heo, N. R. Ko, M. S. Bae, S. J. Lee, B. J. Choi, J. H. Kim, H. K. Kim, S. A. Park and I. K. Kwon, Novel 3D Printed Alginate–BFP1 Hybrid Scaffolds for Enhanced Bone Regeneration, *J. Ind. Eng. Chem.*, 2017, **45**, 61–67, DOI: 10.1016/j.jiec.2016.09.003.

31 S. J. Lee, J. E. Won, C. Han, X. Y. Yin, H. K. Kim, H. Nah, I. K. Kwon, B. H. Min, C. H. Kim, Y. S. Shin, *et al.*, Development of a Three-Dimensionally Printed Scaffold Grafted with Bone Forming Peptide-1 for Enhanced Bone Regeneration with in Vitro and in Vivo Evaluations,

J. Colloid Interface Sci., 2019, **539**, 468–480, DOI: 10.1016/j.jcis.2018.12.097.

32 W. Zhi, X. Wang, D. Sun, T. Chen, B. Yuan, X. Li, X. Chen, J. Wang, Z. Xie, X. Zhu, *et al.*, Optimal Regenerative Repair of Large Segmental Bone Defect in a Goat Model with Osteoinductive Calcium Phosphate Bioceramic Implants, *Bioact. Mater.*, 2022, **11**, 240–253, DOI: 10.1016/j.bioactmat.2021.09.024.

33 M. E. Kim, J. K. Seon, J. Y. Kang, T. R. Yoon, J. S. Lee and H. K. Kim, Bone-Forming Peptide-4 Induces Osteogenic Differentiation and VEGF Expression on Multipotent Bone Marrow Stromal Cells, *Front. Bioeng. Biotechnol.*, 2021, **9**, 1–8, DOI: 10.3389/fbioe.2021.734483.

34 K. Okada, N. Kawao, M. Yano, Y. Tamura, S. Kurashimo, K. Okumoto, K. Kojima and H. Kaji, Stromal Cell-Derived Factor-1 Mediates Changes of Bone Marrow Stem Cells during the Bone Repair Process, *Am. J. Physiol.: Endocrinol. Metab.*, 2016, **310**, E15–E23, DOI: 10.1152/ajpendo.00253.2015.

35 F. Yang, F. Xue, J. Guan, Z. Zhang, J. Yin and Q. Kang, Stromal-Cell-Derived Factor (SDF) 1-Alpha Overexpression Promotes Bone Regeneration by Osteogenesis and Angiogenesis in Osteonecrosis of the Femoral Head, *Cell. Physiol. Biochem.*, 2018, **46**, 2561–2575, DOI: 10.1159/000489684.

36 Y. Liu and B. R. Olsen, Distinct VEGF Functions During Bone Development and Homeostasis, *Arch. Immunol. Ther. Exp.*, 2014, **62**, 363–368, DOI: 10.1007/s00005-014-0285-y.

37 J. Street and B. Lenehan, Vascular Endothelial Growth Factor Regulates Osteoblast Survival – Evidence for an Autocrine Feedback Mechanism, *J. Orthop. Surg. Res.*, 2009, **4**, 19, DOI: 10.1186/1749-799X-4-19.

38 Y. Watanabe, N. Harada, K. Sato, S. Abe, K. Yamanaka and T. Matushita, Stem Cell Therapy: Is There a Future for Reconstruction of Large Bone Defects?, *Injury*, 2016, **47**, S47–S51, DOI: 10.1016/S0020-1383(16)30012-2.

39 P. Su, Y. Tian, C. Yang, X. Ma, X. Wang, J. Pei and A. Qian, Mesenchymal Stem Cell Migration during Bone Formation and Bone Diseases Therapy, *Int. J. Mol. Sci.*, 2018, **19**, 2343, DOI: 10.3390/ijms19082343.

40 J. Li, H. Chen, D. Zhang, J. Xie and X. Zhou, The Role of Stromal Cell-Derived Factor 1 on Cartilage Development and Disease, *Osteoarthrotic Cartilage*, 2021, **29**, 313–322, DOI: 10.1016/j.joca.2020.10.010.

41 F. Bustos, H. Sepúlveda, C. P. Prieto, M. Carrasco, L. Díaz, J. Palma, J. Lattus, M. Montecino and V. Palma, Runt-Related Transcription Factor 2 Induction During Differentiation of Wharton's Jelly Mesenchymal Stem Cells to Osteoblasts Is Regulated by Jumonji AT-Rich Interactive Domain 1B Histone Demethylase, *Stem Cells*, 2017, **35**, 2430–2441, DOI: 10.1002/stem.2704.

42 J. Jeon, M. S. Lee and H. S. Yang, Differentiated Osteoblasts Derived Decellularized Extracellular Matrix to Promote Osteogenic Differentiation, *Biomater. Res.*, 2018, **22**, 4, DOI: 10.1186/s40824-018-0115-0.

43 X. Lin, S. Patil, Y.-G. Gao and A. Qian, The Bone Extracellular Matrix in Bone Formation and Regeneration, *Front. Pharmacol.*, 2020, **11**, 1–15, DOI: 10.3389/fphar.2020.00757.

44 Q. Liu, M. Li, S. Wang, Z. Xiao, Y. Xiong and G. Wang, Recent Advances of Osterix Transcription Factor in Osteoblast Differentiation and Bone Formation, *Front. Cell Dev. Biol.*, 2020, **8**, 1–15, DOI: 10.3389/fcell.2020.601224.

45 A. Grosso, M. G. Burger, A. Lunger, D. J. Schaefer, A. Banfi and N. Di Maggio, It Takes Two to Tango: Coupling of Angiogenesis and Osteogenesis for Bone Regeneration, *Front. Bioeng. Biotechnol.*, 2017, **5**, 1–7, DOI: 10.3389/fbioe.2017.00068.

46 D. Saul, M. M. Menger, S. Ehnert, A. K. Nüssler, T. Histing and M. W. Laschke, Bone Healing Gone Wrong: Pathological Fracture Healing and Non-Unions—Overview of Basic and Clinical Aspects and Systematic Review of Risk Factors, *Bioengineering*, 2023, **10**, 85, DOI: 10.3390/bioengineering10010085.

47 T. K. Ho, J. Tsui, S. Xu, P. Leoni, D. J. Abraham and D. M. Baker, Angiogenic Effects of Stromal Cell-Derived Factor-1 (SDF-1/CXCL12) Variants in Vitro and the in Vivo Expressions of CXCL12 Variants and CXCR4 in Human Critical Leg Ischemia, *J. Vasc. Surg.*, 2010, **51**, 689–699, DOI: 10.1016/j.jvs.2009.10.044.

48 M. Z. Ratajczak, E. Zuba-Surma, M. Kucia, R. Reca, W. Wojakowski and J. Ratajczak, The Pleiotropic Effects of the SDF-1–CXCR4 Axis in Organogenesis, Regeneration and Tumorigenesis, *Leukemia*, 2006, **20**, 1915–1924, DOI: 10.1038/sj.leu.2404357.